

# Quantum clustering and jet reconstruction at the LHC

Jorge J. Martínez de Lejarza<sup>(a)</sup>, Leandro Cieri<sup>(a)</sup> and Germán Rodrigo<sup>(a,b)\*</sup>,

<sup>(a)</sup> Instituto de Física Corpuscular, Universitat de València - Consejo Superior de Investigaciones Científicas, Parc Científic, E-46980 Paterna, Valencia, Spain

<sup>(b)</sup> European Research Council Executive Agency, European Commission, BE-1049 Brussels, Belgium

## Abstract

Clustering is one of the most frequent problems in many domains, in particular, in particle physics where jet reconstruction is central in experimental analyses. Jet clustering at the CERN’s Large Hadron Collider is computationally expensive and the difficulty of this task is expected to increase with the upcoming High-Luminosity LHC (HL-LHC). In this paper, we study the case in which quantum computing algorithms might improve jet clustering by considering two novel quantum algorithms which may speed up the classical jet clustering algorithms. The first one is a quantum subroutine to compute a Minkowski-based distance between two data points, whereas the second one consists of a quantum circuit to track the maximum into a list of unsorted data. The latter algorithm could be of value beyond particle physics, for instance in statistics. When one or both of these algorithms are implemented into the classical versions of well-known clustering algorithms (**K-means**, Affinity Propagation and  $k_T$ -jet) we obtain efficiencies comparable to those of their classical counterparts. Even more, we achieve an exponential speed-up in data dimensionality, when the distance algorithm is applied and an exponential speed-up in data length, when the maximum is selected through the quantum routine.

---

\*Disclaimer: the views expressed are purely those of the writer and may not in any circumstances be regarded as stating an official position of the European Commission.

# 1 Introduction

Quantum computing devices, which are based on the laws of quantum mechanics, offer the possibility to efficiently solve specific problems that become very complex or even unreachable for classical computers since they scale either exponentially or super-polynomially. Algorithms used in quantum computers [1] exploit the quantum principles of superposition and entanglement to clearly manifest a speed-up advantage over the classical counterpart algorithms. Two examples of these quantum algorithms are the well-known cases of Grover’s database querying [2] and Shor’s factoring of integers into primes [3]. These two quantum methods shown, for first time in the 1990s, a clear potential advantage over their corresponding classical analogues. In the past recent years, we have witnessed an impressively fast development of quantum computing algorithms going from optimization problems such as portfolios in fintech [4], applications in quantum chemistry [5], nuclear physics and Monte Carlo simulation [6–8], combinatorial optimization [9], to state diagonalization [10, 11].

Very recently, quantum algorithms have started to be applied in solving problems which appear in high-energy particle physics <sup>1</sup> (HEP). The data already taken at the CERN’s Large Hadron Collider (LHC) and its upcoming Run 3 (which is scheduled to start in the spring of 2022) demand intense data analysis routines and very precise theoretical predictions [13] which are computationally very expensive. This situation will be even more challenging in the posterior high-luminosity phase of the LHC (HL-LHC) [14] and the planned future colliders [15–17]. Recent applications of quantum algorithms to HEP cover diverse subareas such as jet clustering [18–20], jet quenching [21], determination of parton densities [22], simulation of parton showers [23–25], heavy-ion collisions [26], quantum machine learning [27–34], lattice gauge theories [35–38] and multi-loop Feynman integrals [39, 40].

In the present paper we address the problem of clustering and jet reconstruction from collision data, which is a nontrivial and computationally expensive task, as it often involves performing optimizations over potentially large numbers of final-state particles. We consider the possibility of using quantum algorithms to improve the velocity in jet identification. Here we focus on three well-known classical algorithms: the **K-means** clustering [41], the Affinity Propagation (AP) algorithm [42] and the  $k_T$ -jet clustering method in all its variants [43–45]. We propose the corresponding quantum versions of the precedents algorithms: quantum **K-means** clustering, quantum AP-algorithm and quantum  $k_T$ -based algorithms.

Clustering is one of the most frequent classic problems in machine learning and computational geometry. It is a major data analysis tool used in such domains as marketing research, data mining, bioinformatics, image processing, pattern recognition and also in HEP. The popular **K-means** formulation [46, 47], which is a method of vector quantization originally proposed for signal processing, involves the partition of  $n$  observations into  $K$  clusters in which each observation belongs to the cluster with the nearest mean (cluster center or cluster centroid), serving as a prototype of the cluster. Solving this problem exactly is NP-hard <sup>2</sup> (Non-deterministic Polynomial-time hardness), even with just two clusters [48]. Forty years ago, Lloyd [41] proposed a local search solution that is still very widely used today. Usually referred to simply as **K-means**, Lloyd’s algorithm begins with  $K$  arbitrary centers, typically chosen uniformly at random from the data points. Each point is then assigned to the nearest center, and each center is recomputed as the center of all points assigned to it. These two steps (assignment and center calculation) are repeated

---

<sup>1</sup>For a recent review on the applications of quantum computing to data analysis in HEP we refer the reader to Ref. [12] and references therein.

<sup>2</sup>NP-hard problems are not solvable in polynomial time but can be verified in polynomial time.

until the process stabilizes.

The improved version of the **K-means** method, the **K-means++** algorithm [49], initializes the **K-means** algorithm by choosing random starting centers with very specific probabilities. This strategy outperforms **K-means** in terms of both accuracy and speed, often by a substantial margin [49]. The classical **K-means** algorithm was applied to jet clustering in Refs. [50–52]. **K-means** is a method of cluster analysis using a pre-specified number of clusters. It requires an advance (*a priori*) knowledge of  $K$  and belongs to the group of the so-called *partitional clustering algorithms*.

The **AP** algorithm, is a clustering method that identifies representative examples (exemplars) within a given dataset by exchanging messages between all data points. Points are then grouped with their most representative exemplar to give the final set of clusters. The **AP** algorithm was successfully applied to a wide range of problems including face recognition, gene identification, putative exons using microarray data, etc. In Ref. [42], it was shown that the **AP** is faster and more accurate than the **K-means** [46, 47] clustering algorithm. The **AP** algorithm is solid and well understood and the number of clusters is not needed to be pre-specified. Among its disadvantages, we can cite the high time complexity, which turns out to make it not suitable for very large datasets, and the clustering result is typically sensitive to the parameters involved in the **AP** algorithm.

Hierarchical clustering also known as hierarchical cluster analysis (HCA) is also a method of cluster analysis that seeks to build a hierarchy of clusters without having an *a priori* fixed number of clusters. The  $k_T$ -based algorithms [53] belong to the hierarchical category, which needs a linkage function that defines the distance between any two sub-sets (and relies on the base distance between elements). It is the most widely used jet clustering algorithm in the LHC experiments.

The quantum **K-means** clustering algorithm was presented in Refs. [19, 54] for HEP. An earlier study of the quantum **K-means** can be found in Ref. [55]. Both implementations make use of the Euclidean distance to perform the clustering of particles. In this paper, we present a version of the quantum **K-means** clustering algorithm which is based on the definition of a Minkowskian distance at the quantum level for the first time. Considering the case of the quantum version of the **AP** algorithm, it uses the invariant sum squared as a metric in the similarity matrix and calculates it through a quantum subroutine with a similar procedure as in the quantum **K-means** implementation. Regarding the quantum  $k_T$ -based algorithms, to our knowledge, it is the first time it has been presented in the literature. In addition, the search for the maximum distance used in our implementation is performed with a new quantum algorithm. This new quantum method is presented in a general way, and we comment on its reach regarding other areas of interest. Beyond the specific application to jet clustering, the quantum algorithms presented in this paper are of interest to the particle physics and quantum computing communities.

This paper is organized as follows. In Section 2 we introduce our notation and we define the Euclidean and Minkowskian quantum distances. In Section 3 we present our new quantum algorithm in order to search the maximum in a set of a given number of elements. We consider the quantum version of the **K-means** clustering, **AP** and  $k_T$ -based algorithms in Section 4. In Section 5 we present our results considering the quantum simulations of these algorithms and a proof-of-concept implementation with Gaussian datasets as well as with simulated LHC physical events. We also compare their performance in detail. We discuss their differences and conceptual similarities and we compare them with their classical counterparts. A brief summary of our results is presented in Section 6.

## 2 Quantum distances

In quantum computing, it is essential to have the ability to measure quantum entanglement between two states, as in many cases it determines the possibility of obtaining a quantum advantage [56]. We rely on the *SwapTest* method [57] (see Appendix A for more details) in order to probe the entanglement between two given states. The definition of quantum distances (Euclidean distance or Minkowski invariant sum squared presented in this Section, makes use of the *SwapTest* procedure.

### 2.1 Euclidean quantum distance

We start by considering  $N$  data points or vectors in an Euclidean  $d$ -dimensional space,  $\{\mathbf{x}_i\}_{i=1,\dots,N}$ , which are encoded as quantum states of the form

$$|x_i\rangle = |\mathbf{x}_i|^{-1} \sum_{\mu=1}^d x_{i,\mu} |\mu\rangle , \quad (1)$$

where  $|\mathbf{x}_i| = \sqrt{\sum_{\mu=1}^d (x_{i,\mu})^2}$  is the modulus of the vector  $\mathbf{x}_i$ , and  $x_{i,\mu}$  are its components. Each vector requires  $n \geq \log_2 d$  qubits to be encoded, i.e. for  $d = 3$  we need two entangled qubits where one of its states remains free and is not used. The Euclidean distance between two vectors  $\mathbf{x}_i$  and  $\mathbf{x}_j$  is defined classically as

$$d_E^{(C)}(\mathbf{x}_i, \mathbf{x}_j) = |\mathbf{x}_i - \mathbf{x}_j| , \quad (2)$$

where the subscript  $E$  stands for Euclidean and the superscript  $C$  denotes that it corresponds to the classical version.

The quantum analogue of Eq. (2) is obtained by using the controlled *SwapTest* method. In order to define the Euclidean quantum distance between the  $d$ -dimensional vectors  $\mathbf{x}_i$  and  $\mathbf{x}_j$ , we entangle the corresponding associated quantum states  $|x_i\rangle$  and  $|x_j\rangle$ , and define the following subsidiary states

$$|\psi_1\rangle = \frac{1}{\sqrt{2}} (|0, x_i\rangle + |1, x_j\rangle) , \quad |\psi_2\rangle = \frac{1}{\sqrt{Z_{ij}}} (|\mathbf{x}_i||0\rangle - |\mathbf{x}_j||1\rangle) , \quad (3)$$

where  $Z_{ij} = |\mathbf{x}_i|^2 + |\mathbf{x}_j|^2$  is a normalization factor and  $|0\rangle$  and  $|1\rangle$  are the states of an ancillary qubit. It is also convenient to define the swapped state  $|\psi'_1\rangle$

$$|\psi'_1\rangle = \frac{1}{\sqrt{2}} (|x_i, 0\rangle + |x_j, 1\rangle) . \quad (4)$$

The inner products between the quantum states defined in Eqs. (3) and (4) are written as follows

$$\langle \psi'_1 | \psi_2 \rangle = \frac{1}{\sqrt{2Z_{ij}}} (|\mathbf{x}_i| \langle x_i | - |\mathbf{x}_j| \langle x_j |) , \quad \langle \psi_2 | \psi_1 \rangle = \frac{1}{\sqrt{2Z_{ij}}} (|\mathbf{x}_i| |x_i\rangle - |\mathbf{x}_j| |x_j\rangle) . \quad (5)$$

From where

$$\langle \psi'_1 | \psi_2 \rangle \langle \psi_2 | \psi_1 \rangle = \frac{1}{2Z_{ij}} |\mathbf{x}_i - \mathbf{x}_j|^2 . \quad (6)$$

Therefore (see Eq. (24) in Appendix A), the Euclidean quantum distance is

$$d_E^{(Q)}(\mathbf{x}_i, \mathbf{x}_j) = \sqrt{2Z_{ij}(2P_{\Psi_3}(|0\rangle) - 1)} , \quad (7)$$

where the superscript  $Q$  refers to the *Quantum* version of the distance  $d_E$  and the subscript  $\Psi_3$  in the probability  $P$ , means that it is considered the resulting probability of measuring the ancillary qubit in the state  $|0\rangle$  in the last of the three steps in the *SwapTest* procedure.

## 2.2 Quantum invariant sum squared in Minkowski space

Vectors in high-energy physics are defined in a four-dimensional space-time with Minkowski metric. They have the form  $x_i = (x_{i,0}, \mathbf{x}_i)$ , where  $x_{i,0}$  is the temporal component and  $\mathbf{x}_i$  represent the three spacial components. We shall define the analogue of the Euclidean classical distance in the Minkowski space corresponding to the invariant sum squared  $s_{ij}^{(C)}$ , which is commonly called invariant mass squared when vectors are particle four-momenta,

$$s_{ij}^{(C)} = (x_{0,i} + x_{0,j})^2 - |\mathbf{x}_i + \mathbf{x}_j|^2. \quad (8)$$

This quantity, which is Lorentz invariant, can be used as test distance to measure similarity between particle momenta. It is also equivalent to the distance used in some of the traditional jet-clustering algorithms at  $e^+e^-$  colliders [58–60]. It is necessary to apply twice the *SwapTest* subroutine (presented in Appendix A) for computing the Minkowski-type distance through a quantum algorithm. Once for the spatial and other for temporal components.

The spatial distance is computed through the procedure explained in the previous section with a slight modification with respect to Eq. (5) (change of sign in the term proportional to qubit  $|1\rangle$ )

$$|\psi_2\rangle \longrightarrow |\psi_2\rangle = \frac{1}{\sqrt{Z_{ij}}} (|\mathbf{x}_i||0\rangle + |\mathbf{x}_j||1\rangle), \quad (9)$$

whereas the temporal part is computed as a result of the overlap of the following states:

$$|\varphi_1\rangle = H|0\rangle = \frac{1}{\sqrt{2}} (|0\rangle + |1\rangle), \quad |\varphi_2\rangle = \frac{1}{\sqrt{Z_0}} (x_{0,i}|0\rangle + x_{0,j}|1\rangle), \quad (10)$$

where  $Z_0 = x_{0,i}^2 + x_{0,j}^2$ . Then, applying the *SwapTest* to these states one gets the relation:

$$P(|0\rangle|_{time}) = \frac{1}{2} + \frac{1}{2} |\langle \varphi_1 | \varphi_2 \rangle|^2, \quad (11)$$

where the overlap  $|\langle \varphi_1 | \varphi_2 \rangle|^2$  is trivially given by

$$|\langle \varphi_1 | \varphi_2 \rangle|^2 = \frac{1}{2Z_0} (x_{0,i} + x_{0,j})^2. \quad (12)$$

Therefore:

$$(x_{0,i} + x_{0,j})^2 = 2Z_0 (2P_{\Psi_3}(|0\rangle|_{time}) - 1). \quad (13)$$

At this point, the quantum version of the invariant sum squared follows from the combination of results from Eq. (7) and Eq. (13):

$$s_{ij}^{(Q)} = 2(Z_0(2P_{\Psi_3}(|0\rangle|_{time}) - 1) - Z_{ij}(2P_{\Psi_3}(|0\rangle|_{spatial}) - 1)). \quad (14)$$

The quantum circuit used to implement the invariant sum-squared distance is shown in Fig. 1. In the first step (until the first barrier in Fig. 1) the states  $|x\rangle$  and  $|y\rangle$  are encoded in the  $n$ -dimensional second and third wires. Then, a CSWAP gate is applied and the state  $\psi_1$  is encoded in the first and second wires, whereas the third row is left with unusable information. In the second step, the third wire is re-initialized to vector  $|0\rangle^{\otimes n}$  with the inverse unitary gates of step one leaving the first wire invariant. Subsequently, in the third step, the state  $\psi_2$  is encoded into the first qubit of the third wire and the *SwapTest* is applied to measure the spatial part. Contemporaneously, the states  $\varphi_1$  and  $\varphi_2$  are encoded into the 3<sup>rd</sup> and the 4<sup>th</sup> qubits of the third wire and another *SwapTest* is applied to measure the temporal part. Notice that if  $n < 5$  we must use new qubits instead of reusing those from the third  $n$ -dimensional wire.

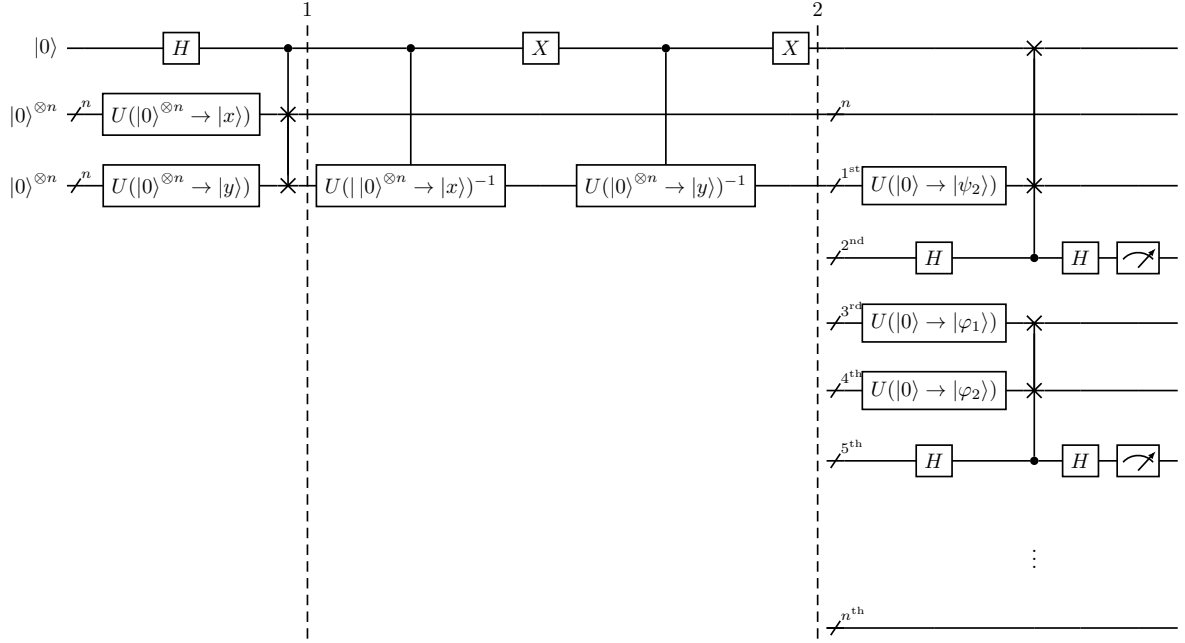


Figure 1: Quantum circuit to obtain the invariant sum squared between two  $d$ -dimensional vectors using  $n = \log_2(d - 1)$  qubits to encode each of them. Note that from the second barrier onward the third  $n$ -dimensional wire splits into multiple one-dimensional wires.

### 3 Quantum maximum search by amplitude encoding

Finding a particular member belonging to a dataset is a recurring problem in data analysis. This is a computationally very expensive task. However, quantum computing offers suitable tools to solve data query in a shorter computational time. In particular, it is well known the quadratic speed up exhibited by Grover's algorithm [2]. In this paper, we present a considerably simpler algorithm that is used exclusively to find the maximum in a list of values. This algorithm, although very elementary, is sufficiently accurate for the applications that we will present in Sections 5.1 and 5.3. To our knowledge, it is the first time presented in the literature.

Let  $L[0, \dots, N - 1]$  be an unsorted list of  $N$  items. Solving the maximum searching problem is to find the index  $y$  such that  $L[y]$  is the maximum. The quantum algorithm to solve that problem using amplitude encoding proceeds in two steps:

1. The list of  $N$  elements is encoded into a  $\log_2(N)$  qubits state as follows:

$$|\Psi\rangle = \frac{1}{\sqrt{L_{sum}}} \sum_{j=0}^{N-1} L[j] |j\rangle, \quad (15)$$

where  $L_{sum} = \sum_{j=0}^{N-1} L[j]^2$  is a normalization constant. This amplitude encoding is achieved using  $U$  and CNOT quantum gates (see Fig. 2).

2. The final state is measured. This step is rerun several times to reduce the statistical uncertainty. Once done, the most repeated state gives us the maximum.

The graphical representation of the algorithm is shown in Fig. 2, where  $n = \log_2(N)$  qubits are needed to encode a list of  $N$  (real) elements <sup>3</sup>.

<sup>3</sup>Complex elements can be encoded with a similar circuit. However, it would take a few more quantum gates.

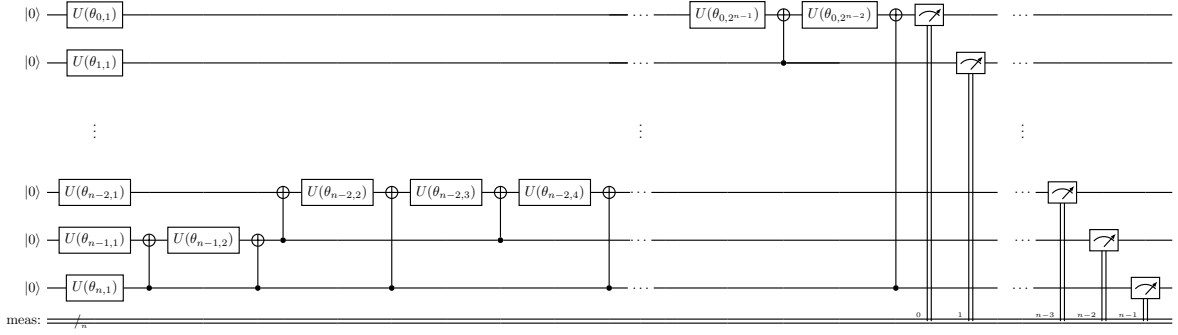


Figure 2: Quantum circuit for quantum maximum searching by amplitude encoding.

The quantum algorithm proposed in this paper is  $\mathcal{O}(\log(N))$ . The bottleneck of this procedure underlies in encoding data into a quantum state. When data is stored in a quantum random access memory (qRAM), encoding takes  $\mathcal{O}(\log_2(N))$  steps [61–68]. The corresponding classical algorithms typically used to obtain the minimum of an unsorted list of  $N$  items are of order  $\mathcal{O}(N)$ . Therefore the improvement introduced by our quantum algorithm is exponential.

The well-known quantum minimum searching algorithm proposed by Dürr and Høyer [69] is  $\mathcal{O}(\sqrt{N})$ . After their theoretical paper [69] the algorithm was studied and implemented in a quantum simulator (see Ref. [70]). In summary, previous implementations [70] of the Dürr and Høyer algorithm suggests that it could be improved, given the excessive number of qubits needed to implement the method, the unviability to hard code a different oracle for each element, the large number of *shots* required and (in some cases) the poor performance obtained. This is the aim of the new quantum maximum searching algorithm by amplitude encoding presented here: the improvement of the previous enumerated challenges.

Nevertheless, the new algorithm presented in this paper and the corresponding Dürr and Høyer quantum method share common features that could lead to miss-identification of the respective absolute maximum and minimum. These cases, in which the list typically presents a very low standard deviation (or the largest/minimum values are very close to each other) could manifest difficulties related to the fact that the probability of measuring several candidates would be almost identical.

Regarding the practical implementation of the quantum algorithm presented in this paper, the results shown in Section 5 reveal that these potential difficulties do not manifest strongly in the context of jet clustering.

Beyond the jet clustering procedure in HEP, there are other fields where our quantum algorithm could be of value. For instance, in the so-called Extreme Value Theory (EVT) [71]. According to Gumbell 1958 [72], this particular field studies the probability distribution of the desired data by focusing on the outliers with the ultimate goal of being able to predict them in the future. It is precisely in this estimation of the extreme values where our algorithm could be useful. Since for the predictive models historical data has to be analysed and therefore extreme values have to be searched in large data lists. This would mean that our algorithm could be implemented successfully in statistical analysis of extreme data, including actuarial and financial sciences, meteorology, material sciences, engineering and environmental sciences climatology, geology, hydrology and highway traffic analysis [73–75].

## 4 Quantum clustering algorithms

### 4.1 K-means algorithm

**K-means** is an unsupervised machine learning algorithm that classifies the elements of a dataset into  $K$  groups called clusters [46, 47]. The data points within each cluster have to be as similar (near) as possible whereas the clusters themselves have to be as different (far) as possible from each other. The input for this algorithm is a set of  $N$  data points or vectors, in  $d$  dimensions as well as the number of clusters  $K$ , with  $K \leq N$ , and its output is a set of  $K$  centroids, calculated by averaging the position of the data points corresponding to each group, thus defining  $K$  clusters. The flow chart of this algorithm is the following:

1.  $K$  initial centroids within the data points are generated. They can be generated randomly or through a specific method such as *kmeans++* [49].
2. Each data point is assigned to its closest centroid according to a distance that has been defined in advance, thus the  $K$  clusters are defined. The most commonly used distance is the Euclidean distance.
3. Each centroid is recalculated by averaging the associated data points.
4. Steps 2 and 3 are repeated until all centroids stabilize and convergence is achieved.

This **K-means** algorithm has a sophisticated quantum version that differs from its classical counterpart in two points [76]. First, the quantum **K-means** introduces a quantum method to calculate the distance between data points. Second, the quantum version also includes a procedure for obtaining the minimum distance of each data point with respect to the  $K$  centroids, which is achieved by Dürr and Høyer's algorithm [69].

In this paper, we focus on a new quantum version of the **K-means** algorithm, where the calculation of distances is made quantumly and the minimum distance of each data point to the centroids is obtained with the quantum maximum searching algorithm<sup>4</sup> explained in Section 3. Other quantum versions of the **K-means** algorithm have been studied in Refs. [19, 54] and [55], where an Euclidean distance was used to separate the particles from each other. In this paper, we analyse for the first time an implementation of the **K-means** algorithm with a Minkowski-type quantum distance, as defined in Section 2.2.

The time complexity of this algorithm is estimated by analysing the time complexity of its components. The distances that have to be calculated are  $\mathcal{O}(N)$ , the search of a minimum distance for every data point with respect to the centroids is  $\mathcal{O}(\log K)$ , and the calculation of each distance itself requires  $(1+2\log_2(d-1))$  qubits<sup>5</sup>. Since neither the addition nor the multiplication constants contribute to the total time complexity, this step only counts asymptotically as  $\mathcal{O}(\log(d-1))$ . This results in a speedup from  $\mathcal{O}(NKd)$  in the classical version to  $\mathcal{O}(N \log K \log(d-1))$  in our quantum version. Therefore an exponential speed-up in the number of clusters and in the vector dimensionality is achieved. A quantum simulation of the quantum **K-means** algorithm is presented in Section 5.1.

---

<sup>4</sup>We may apply this algorithm for finding the minimum since obtaining the minimum amongst the distances is equivalent to obtaining the maximum of its inverses:  $s_{ij}^{-1}$ .

<sup>5</sup>It is necessary an ancillary qubit and  $2\log_2(d-1)$  qubits to encode the temporal and the spatial parts, respectively.

## 4.2 Affinity Propagation algorithm

Although **K-means** is a successful algorithm capable of clustering data in a satisfactory manner, it needs the number of clusters  $K$  to be defined beforehand, which is not typically the case in HEP applications. The Affinity Propagation (AP) algorithm [42], which is an unsupervised machine learning algorithm, does not need the number of clusters as an input. AP only takes as input the data points that have to be classified. So, let  $x_1, \dots, x_N$  be a set of data points. Then, a function  $s$  to quantify the similarity between points is computed. In such a way that  $s(i, j) \geq s(i, k)$  if and only if  $x_i$  is more similar to  $x_j$  than to  $x_k$ . The most common metrics to measure the similarity is the negative squared distance of the two points we are comparing:  $s(i, j) = -|x_i - x_j|$ . The diagonal  $s(i, i)$  of the matrix  $s$  is especially relevant since it stores values referred as “preferences” that are related to how likely a particular instance is to become an exemplar, i.e, a cluster. Most of the metrics make the diagonal  $s(i, i)$  be  $s(i, i) = 0, \forall i \leq N$ , although it can be different from 0. Hence, on the first iteration, every element  $s(i, i)$  is set to the same certain value, which is typically the median similarity of all pairs of inputs. Next, two matrices are calculated that are related to the concept of message exchanging between data points [42]. First, there is the responsibility matrix  $R$ . This matrix contains the values  $r(i, k)$  that quantify the suitability of point  $k$  to serve as the exemplar for point  $i$ , compared to other candidate exemplars for  $i$ . Then comes the availability matrix  $A$ , whose elements  $a(i, k)$  reflect how appropriate it would be for point  $i$  to select point  $k$  as its exemplar, relative to the preferences of other points for  $k$  as an exemplar. As they have been described, both matrices could be viewed as log-probability ratios. Then, the AP flow chart reads:

1. The matrices  $R$  and  $A$  are initialized to zero.
2. The responsibility matrix is computed:

$$r(i, k) = s(i, k) - \max_{q \neq k} \{a(i, q) + s(i, q)\}. \quad (16)$$

3. The availability matrix is computed:

$$a(i, k) = \min \left( 0, r(k, k) + \sum_{q \notin \{i, k\}} \max(0, r(q, i)) \right) \text{ for } i \neq k, \text{ and} \quad (17)$$

$$a(k, k) = \sum_{q \neq k} \max(0, r(q, k)). \quad (18)$$

4. Steps 2 and 3 are repeated until either the cluster boundaries remain unchanged for several iterations, or a predetermined number (of iterations) is reached.

Once convergence has been reached, the exemplars i.e, the clusters, are obtained from the final matrices as those whose  $r(i, i) + a(i, i) > 0$ . This algorithm takes  $\mathcal{O}(N^2)$  steps to fill the similarity matrix, and also computing each element takes  $\mathcal{O}(d)$ , since a distance between two  $d$ -dimensional points has to be calculated. Moreover, steps 2 and 3 are repeated a number  $T$  of times, so the final time complexity of this algorithm is  $\mathcal{O}(N^2 T d)$ .

Here, a quantum (hybrid) algorithm is presented which uses the invariant sum squared as a metric in the similarity matrix and calculates it through a quantum subroutine, as the **K-means** algorithm described in the subsection 4.1. Then, a speedup is achieved, since computing the distances only requires  $(1 + 2 \log_2(d - 1))$  qubits. So, the quantum AP algorithm, which is as far as we know completely original, has a time complexity of  $\mathcal{O}(N^2 T \log(d - 1))$ .

### 4.3 Generalised $k_T$ -jet algorithm

The inclusive variant of the generalised  $k_T$ -jet algorithm is formulated as follows [53]:

1. For each pair of partons  $i, j$  the following distance is computed:

$$d_{ij} = \min(p_{T,i}^{2p}, p_{T,j}^{2p}) \Delta R_{ij}^2 / R^2, \quad (19)$$

with  $\Delta R_{ij}^2 = (y_i - y_j)^2 + (\phi_i - \phi_j)^2$ , where  $p_{T,i}$ ,  $y_i$  and  $\phi_i$  are the transverse momentum (with respect to the beam direction), rapidity and azimuth of particle  $i$ .  $R$  is a jet-radius parameter usually taken of order 1. For each particle  $i$  the beam distance is  $d_{iB} = p_{T,i}^{2p}$ .

2. Find the minimum  $d_{min}$  amongst all the distances  $d_{ij}$ ,  $d_{iB}$ . If  $d_{min}$  is a  $d_{ij}$ , the particles  $i$  and  $j$  are merged into a single particle summing their four-momenta (this is the E-scheme recombination); if  $d_{min}$  is a  $d_{iB}$  then the particle  $i$  is declared as a final jet and it is removed from the list.
3. Repeat from step 1 until there are no particles left.

It is noticeable that for specific values of  $p$  in Eq. (19), the generalised  $k_T$  algorithm is reduced to the algorithms:  $k_T$  ( $p = 1$ ), Cambridge/Aachen ( $p = 0$ ) and anti- $k_T$  ( $p = -1$ ). As it is claimed in Ref. [77], this classical version of the  $k_T$ -jet algorithm is  $\mathcal{O}(N^3)$ , since the bottleneck of the algorithm is scanning the  $\mathcal{O}(N^2)$  table with all the distances  $d_{ij}$ ,  $d_{iB}$ , and it has to be done  $N$  times. Nevertheless, the **FastJet** algorithm is able to reduce the complexity to  $\mathcal{O}(N^2)$ . It is achieved by identifying each particle's geometrical nearest neighbour, thereby it is not necessary to construct a size- $N^2$  table of  $d_{ij}$ , but only the size- $N$  array,  $d_{iG_i}$ , where  $G_i$  is  $i$ 's geometrical nearest neighbour. Furthermore, this **FastJet** algorithm can be optimized further using the so-called Voronoi diagrams achieving a reduction in the time complexity from  $\mathcal{O}(N^2)$  to  $\mathcal{O}(N \log N)$ .

Regarding the quantum version of this algorithm, the distance  $\Delta R_{ij}^2$  will be computed classically whereas the minimum will be obtained through a quantum algorithm. This is due to the fact that the speed up achieved by obtaining the minimum here with a quantum subroutine will be dominant. Thereby, what is to be used here is the new algorithm to obtain the maximum of a list of values (see Section 3). So obtaining the minimum amongst all the distances  $d_{ij}$ ,  $d_{iB}$  will turn out to be obtaining the maximum of its inverses:  $d_{ij}^{-1}$ ,  $d_{iB}^{-1}$ . Actually, these inverse distances are what will be computed directly for each pair  $i, j$ . Since computing the distances and thereafter computing its inverses would require traversing a vector of size  $N$ , so it would have a complexity  $\mathcal{O}(N^2)$ . With that in mind one may also directly compute  $d_{ij}^{-a}$ ,  $d_{iB}^{-a}$ , with  $a \in \mathbb{N}$ , to increase the separation among the data, which makes the maximum more likely when measuring. And this will not increase the overall time complexity of the algorithm either. In Section 5 we compare the results obtained when applying the algorithm with different  $a$  values.

The quantum maximum searching algorithm presented above could be applied to the  $k_T$ -jet algorithm successfully because accuracy is not critical. Even if our quantum algorithm fails to obtain the absolute maximum in one of the multiples iterations, this could end up not affecting the overall jet clustering process. Since an error in finding the maximum will provoke a flip in the order in which two particles merge, and the final result will in many cases be independent of this permutation.

As a final remark, notice that the  $k_T$ -jet quantum algorithm is  $\mathcal{O}(N^2 \log(N))$ , since computing all the distances takes  $\mathcal{O}(N^2)$  and finding the minimum is  $\mathcal{O}(\log(N))$ , in comparison with the  $\mathcal{O}(N^3)$  that requires its classical analogue [77]. Furthermore, the quantum minimum searching could also be implemented in the **FastJet** algorithm of complexity  $\mathcal{O}(N^2)$ . In this case, the

resulting quantum algorithm would be  $\mathcal{O}(N \log(N))$ , which is of the same order as the `FastJet` algorithm version with Voronoi diagrams, which is the most efficient clustering algorithm known to date. This quantum algorithm of order  $\mathcal{O}(N \log(N))$  has been tested in Section 4.3 with LHC physical datasets.

## 5 Quantum simulations

The implementation of the quantum algorithms has been performed through the open-source IBMQ software. In particular, the Python module *Qiskit* developed by IBMQ has been used to build the quantum circuit to calculate the invariant sum squared as described in section 2.2 for the **K-means** and the **AP** algorithm, as well as to build the quantum circuit for finding the minimum distance in the **K-means** and the  $k_T$ -jet algorithm. Afterward, these quantum subroutines have been introduced into their respective classical algorithm substituting the classical part they are speeding up. The *Qiskit* module serves for executing circuits on real quantum devices. Nevertheless, in previous studies such as [55] and [78], it has been found that the experimental error associated with the real machines provided by IBMQ is not yet sufficiently small to extract significant results. Hence, the algorithms presented here have been executed on a quantum simulator that offers an unrestricted and noise-free environment.

### 5.1 Quantum K-means with Minkowski-type distance

At this point we present our implementation of the **K-means** algorithm with the invariant sum squared as a distance as well as a maximum searching algorithm, and compare its performance with its classical analogue. To this end, we have generated 15 Gaussian clustered datasets of  $N = 300$  three-dimensional vectors<sup>6</sup> with different levels of noise and clustering using the *Scikit-learn* function *make\_blobs*, which gives us the *true labels*<sup>7</sup> of the generated data. These *true labels* of the data points are used to calculate the true efficiencies,  $\varepsilon_t$ , of the algorithms when analysing Gaussian datasets. The efficiency  $\varepsilon_t$  is obtained as the ratio of the number of particles classified by the algorithm in the same way as the *true labels* to the total number of particles. We then applied the hybrid and classical versions of the **K-means** algorithm to each dataset. Note that the data we are analysing represent the particle four-momenta in such a way that the three-dimensional vectors correspond to the spatial components, while the temporal components are calculated assuming that all particles are massless and on shell. Results are shown in Figs. 3 and 4.

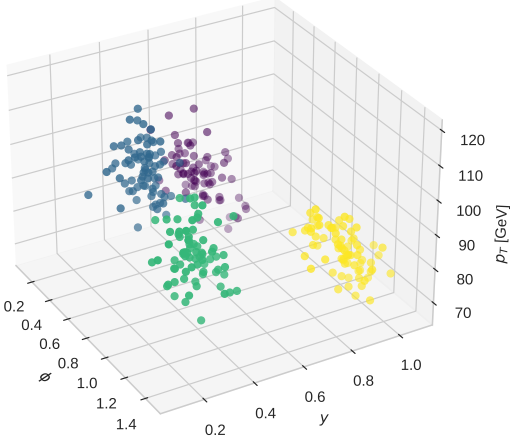
Regarding Fig. 3 one can see at a glance that both classical and quantum versions perform the clustering in the same way in the three-dimensional space of transverse momentum ( $p_T$ ), rapidity ( $y$ ) and azimuth ( $\phi$ ).

Fig. 4 shows the efficiency in the reconstruction of the clusters as a function of the standard deviations used to generate the data, namely we check whether clustering occurs as expected. It is evident that for small values of the standard deviation both algorithms perform really well, with efficiencies close to one, while for larger values of the standard deviation (i.e. highly noisy data) both efficiencies drop. Furthermore, we can compare the performances of the **K-means** algorithm when the seed of the centroids is chosen randomly (see Fig. 4a), with respect to the case when

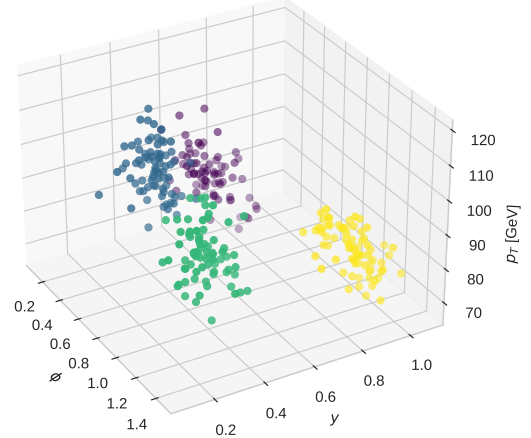
---

<sup>6</sup>In general, it is possible to relate this generated set of three-dimensional vectors, to a physical event at the LHC. It is enough to consider the set of  $n$  three-dimensional vectors as massless partons recoiling against a small number of tagged particles.

<sup>7</sup>The data generator function pre-assigns each data point to a particular cluster, so by analysing these *true labels* one may know which is the correct way to cluster the data.

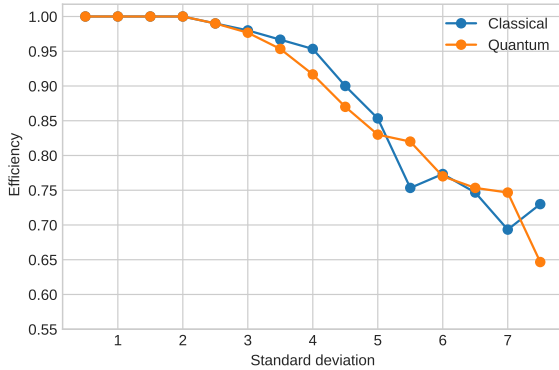


(a) Classical **K-means** clustering,  $\varepsilon_t = 1.00$ .

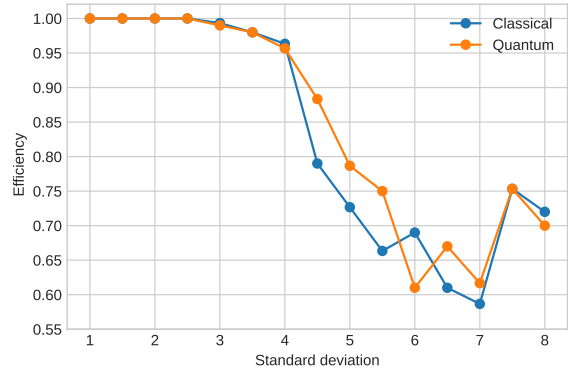


(b) Quantum **K-means** clustering,  $\varepsilon_t = 1.00$ .

Figure 3: In different colors, clusters identified after 5 iterations by the classical and quantum versions of the **K-means** algorithm in a Gaussian dataset generated with a random seed and a standard deviation of 2.0 from the cluster centroids. Note that clusterization has been performed using a Minkowski-type distance assuming that all particles are massless and on shell and the efficiencies of both algorithms are  $\varepsilon_t = 1.00$ .



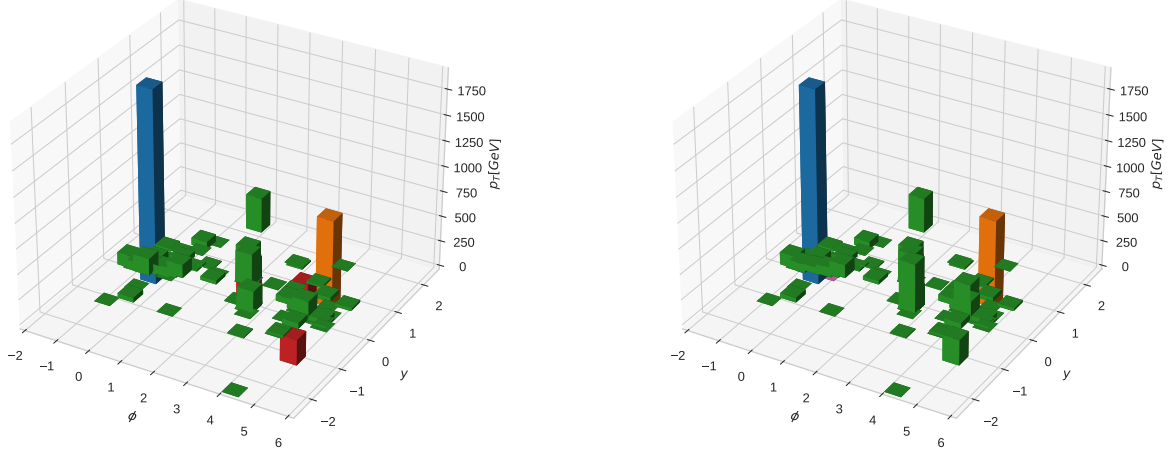
(a) Random seed.



(b) **K-means++** seed.

Figure 4: Cluster efficiency of the **K-means** algorithm versus standard deviations of the data with respect to centroids. Both the classical and quantum versions have been run on 15 datasets with standard deviations ranging from 0.5 to 7.5.

the seed centroids are carefully selected to be as far as possible from each other, according to the **K-means++** prescription (see Fig. 4b). The random seed variant in Fig. 4a, has a linear decrease with respect to the standard deviation, and the performances of classical and quantum versions are very similar. On the other hand, the **K-means++** variant, Fig. 4b, presents a different behaviour. The quantum version outperforms, in the majority of the cases, the classical one from a standard deviation of 4 onward. Furthermore, in this variant both performances show a dropoff from 4 standard deviations to 7, and then a slight rise from 7 to 8. Finally, comparing both variants it is observed that the **K-means++** method outperforms the random seed case for small values of the standard deviation ( $< 4$ ). However, for larger values of the standard deviation the random seed



(a) Classical **K-means** applied to LHC physical events.

(b) Quantum **K-means** applied to LHC physical events,  $\varepsilon_c = 0.94$ .

Figure 5: A sample parton-level event generated as described in the text and clustered with the classical and the quantum version of the **K-means++** algorithm, taking  $K = 8$ .

prescription presents higher efficiencies.

In the following, we will apply our quantum **K-means** method to LHC physical events. To do so we first have processed the data to avoid the following problem: a negative vector  $-\mathbf{x}$  represents the same quantum state  $|x\rangle$  as its positive analogue  $\mathbf{x}$  up to a global phase. This data processing consists of rescaling the data to be analysed in the interval  $\{1,10\}$ <sup>8</sup>. This means every component of every data point will be rescaled in the desired interval. Thus, all the data points are positive now. Moreover, when analysing LHC physical events, we no longer have the *true labels*, so we cannot calculate  $\varepsilon_t$ . Instead, we define the efficiency  $\varepsilon_c$ , which is defined as the quotient of the number of particles clustered in the same way as their classical counterpart and the total number of particles to be classified.

We consider the generation of a physical  $n$ -particle event produced at the LHC. We use a private implementation of an  $n$ -particle ( $n$  can be of the order of tens of thousands) phase-space event generator. This **C++** code, which is based on **ROOT** [79], generates  $n$ -particle events, in which the final-state particles can be massive or massless in any combination of each other (combination chosen by the user). This allows the user to generate final states in which all the particles are massless QCD partons, massless QCD partons associated with photons, massive vector bosons, top-quarks, etc.

The precision in the generation of the final-state event is verified on an event-by-event basis by computing the kinematical constraint between the initial and the  $n$ -particle final state. The required precision <sup>9</sup> is always better than  $10^{-2}$ . Each generated event is then analysed with the

<sup>8</sup>Note that the value 0 is not included to avoid numerical and statistical fluctuations

<sup>9</sup>If we consider all momenta of the event outgoing, the kinematical constraint is evaluated over the resulting three-momentum space vector. The test in the accuracy of the kinematical constraint is performed at the highest multiplicity in the final state. This constitutes the lowest limit for the precision, since reducing the particle number

classical versions of the  $k_T$ -jet algorithms (as implemented in **FastJet** [53]) and with our quantum version of the corresponding jet algorithms.

In this paper we consider the  $n$ -particle massless final-state production in proton-proton <sup>10</sup> collisions at a centre-of-mass energy of  $\sqrt{s} = 14$  TeV. We apply the following final-state selection cuts. We select jets with the  $k_T$ -jet algorithms according to the following parameters: the minimum transverse momentum of the resulting jets is required to be  $p_{T\min} \geq 10$  GeV and with a radius  $R = 1$ . For our study, we consider  $n$  massless particles in the final state with  $n = 128$ .

The application of the quantum **K-means++** method to LHC physical events is displayed in Fig. 5. Notice that even if we choose  $K = 8$  beforehand, one may see in Fig. 5 that the algorithms clearly distinguish only 3 or 4 clusters (jets). There is actually a simple explanation. Although the algorithm starts with  $K$  centroids, the algorithm may converge to a local minimum when the number of clusters is less than  $K$ , leaving the remaining clusters completely empty.

In Fig. 5 one can observe graphically that both algorithms classify the data in much the same way, and also the efficiency shown by the quantum algorithm is close to one. Therefore, the results of this quantum version using physical data may be considered satisfactory.

## 5.2 Quantum Affinity Propagation algorithm

In this subsection, a simulation of the quantum AP algorithm is presented. First, we apply this algorithm to Gaussian datasets with different numbers of clusters, generated with a standard deviation of 0.6. That value of the standard deviation has been chosen arbitrarily by convenience. The efficiencies resulted for the classical and the quantum versions are shown in Table. 1. Table 1 depicts that the AP classical algorithm and its quantum counterpart clustered the low-noise Gaussian datasets successfully.

| Number of clusters $K$ | Efficiency classical AP ( $\varepsilon_t$ ) | Efficiency quantum AP ( $\varepsilon_t$ ) |
|------------------------|---|---|
| 4                      | 1.00  | 0.99                                      |
| 5                      | 1.00  | 1.00                                      |
| 6                      | 0.99  | 0.98                                      |
| 7                      | 1.00  | 0.98                                      |
| 8                      | 0.98  | 0.94                                      |

Table 1: Efficiencies of AP algorithms for Gaussian datasets with different number of clusters.

In the following, we apply this algorithm to the physical dataset described in Section 5.1, which was preprocessed for the reasons explained in the same section. The results obtained are shown in Fig. 6. In Fig. 6b exactly the same clustering is performed as in Fig. 6a (notice that the efficiency of the quantum version is  $\varepsilon_c = 1.00$ ). Nonetheless, this algorithm only finds 2 clusters, which differs with respect to the 3 or 4 clusters found by the **K-means** algorithm (see Fig. 5). Even more, both algorithms identify correctly the most energetic jets of the event (the blue and the orange ones) while the majority of the remaining particles are not classified in the same way, probably because they are soft particles.

in the final state, the precision improves.

<sup>10</sup>Since we are considering unweighted events, our study is not only valid for proton-proton colliders, but also for  $e^+e^-$  colliders.

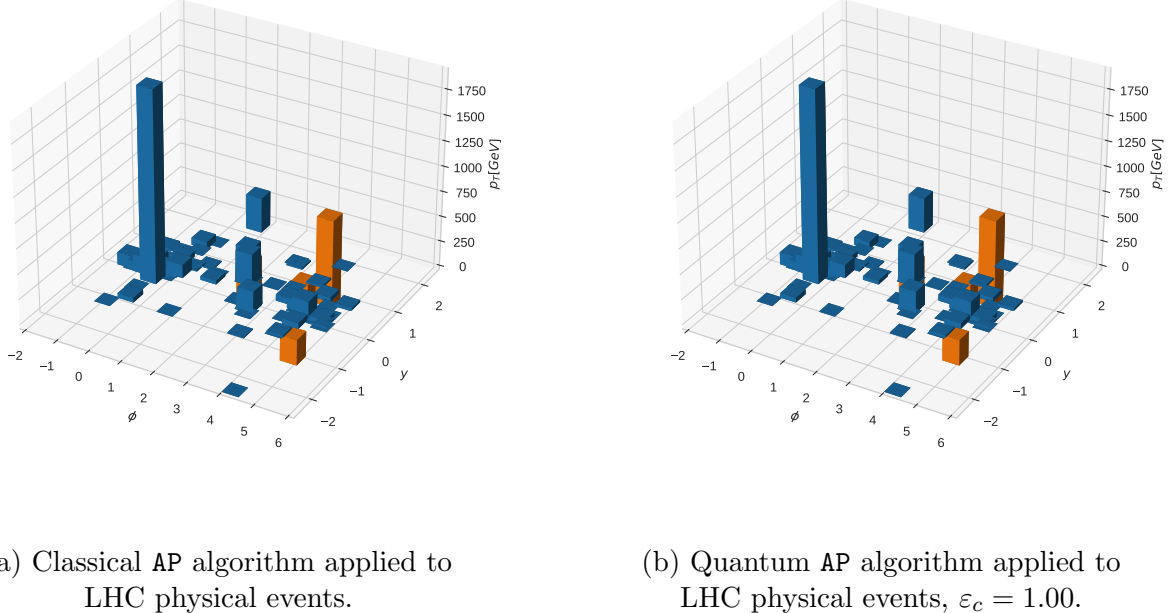


Figure 6: A sample parton-level event generated as described in the text and clustered in  $K = 2$  different clusters with the classical and the quantum version of the AP algorithm.

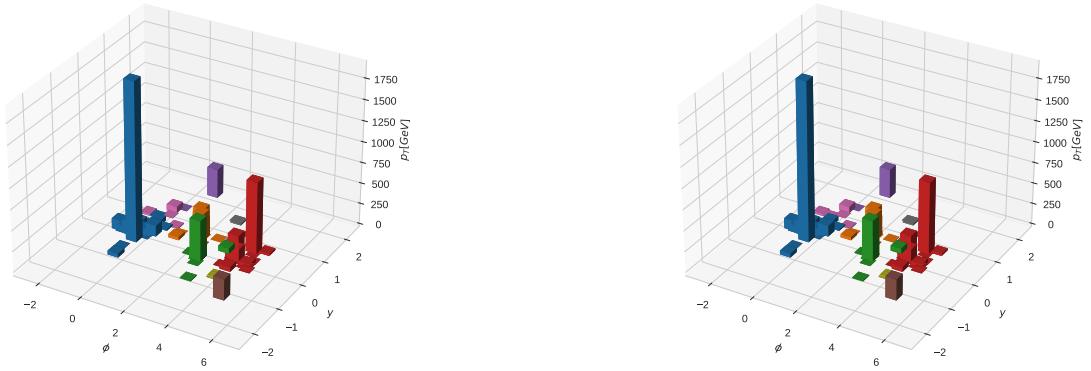
### 5.3 Quantum $k_T$ jet algorithm

In this section, we apply the quantum version of the  $k_T$ -jet algorithm to the same LHC physical events as described in Section 5.1 in order to compare the three clustering algorithms.

In Fig. 7 we show the performance of classical and quantum  $k_T$  jet algorithms. It depicts the jet clustering process carried out by each one of the  $k_T$  algorithm versions, i.e. anti- $k_T$ ,  $k_T$  and Cambridge/Aachen. The classical and quantum versions perform the same jet clustering.

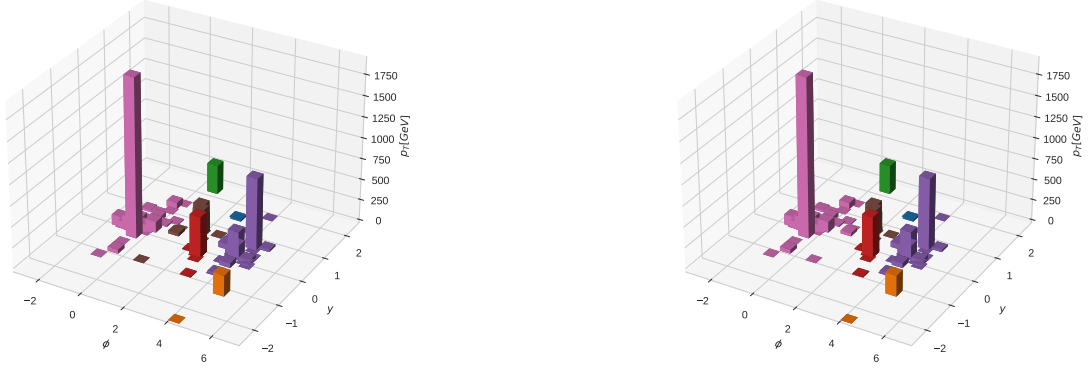
When comparing Figs. 5, 6 and 7, one can observe that the latter performs a cleaner clusterization with a larger number of jets. This is a visual effect because jet clusterization is represented graphically in 3-dimensions, which coincides with the dimensionality of the  $k_T$  metrics, while the K-means and AP use a 4-dimensional Minkowski distance.

To conclude this section we also analyse the efficiencies and the number of *shots* required for all the quantum versions as a function of the  $a$  parameter (see Section 4.3). These are shown in Table 2. Table 2 displays that the efficiencies of the quantum algorithms are close to one, i.e., they classify particles almost identically to their classical counterparts. Furthermore, it may be observed that the larger the parameter  $a$ , the smaller the number of *shots* required to achieve a successful efficiency. In this case, we only need to increase the parameter  $a$  to the number 5 to achieve the desired efficiencies with at most 10 *shots*. However, in other problems (with a larger dataset) a parameter greater than  $a = 5$  can be used to separate the data points and achieve the highest possible efficiency with the smallest number of *shots*.



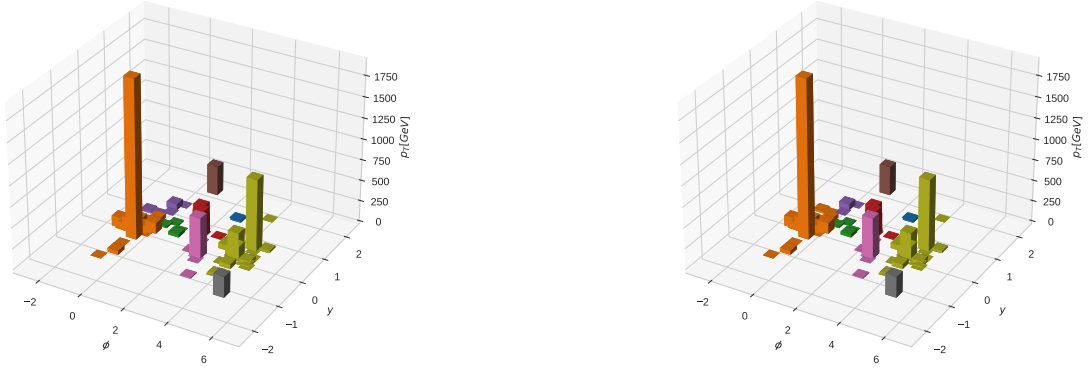
(a) Classical anti- $k_T$ ,  $p = -1$ ,  $R = 1$ .

(b) Quantum anti- $k_T$ ,  $p = -1$ ,  $R = 1$ ,  $\epsilon_c = 0.99$ .



(c) Classical  $k_T$ ,  $p = 1$ ,  $R = 1$ .

(d) Quantum  $k_T$ ,  $p = 1$ ,  $R = 1$ ,  $\epsilon_c = 0.98$ .



(e) Classical Cam/Aachen,  $p = 0$ ,  $R = 1$ .

(f) Quantum Cam/Aachen,  $p = 0$ ,  $R = 1$ ,  $\epsilon_c = 0.98$ .

Figure 7: A sample parton-level event generated as described in the text and clustered with three different  $k_T$ -jets algorithms as well as its quantum versions.

| $a$ | Efficiency<br>anti- $k_T$ | Shots<br>anti- $k_T$ | Efficiency<br>$k_T$ | Shots $k_T$ | Efficiency<br>Cam/Aachen | Shots<br>Cam/Aachen |
|-----|---------------------------|----------------------|---------------------|-------------|--------------------------|---------------------|
| 1   | 0.96                      | 50                   | 0.98                | 50          | 0.96                     | 70                  |
| 2   | 0.99                      | 40                   | 0.99                | 45          | 0.98                     | 60                  |
| 3   | 1.00                      | 25                   | 0.98                | 20          | 0.97                     | 40                  |
| 4   | 1.00                      | 15                   | 0.95                | 15          | 1.00                     | 20                  |
| 5   | 0.99                      | 5                    | 1.00                | 8           | 0.98                     | 10                  |

Table 2: Efficiencies and number of *shots* of the different quantum  $k_T$ -jet algorithms as a function of parameter  $a$ .

## 6 Conclusions

In this paper, we have considered the quantum versions of the well-known **K-means**, Affinity Propagation and  $k_T$ -jet clustering algorithms.

The quantum versions of the jet clustering algorithms presented here are based on two novel quantum procedures. The first one is a quantum subroutine which serves to compute distances satisfying Minkowski metric, whereas the second one consists of a quantum circuit to track the maximum into a list of unsorted data.

In the case of the **K-means** clustering algorithm, the quantum version is based on the standard classical algorithm with a quantum procedure to compute distances in Minkowski space and an additional quantum procedure to assign each particle to the nearest centroid. We found that the **K-means** quantum algorithm has a clustering efficiency as good as its classical counterpart while it showed an exponential speed-up in computational time in the vector dimensionality  $d$ , as well as in the number of clusters  $K$ .

In the second place, we considered a quantum version of the Affinity Propagation method, which is an unsupervised machine learning algorithm, where the similarity is computed with the same quantum procedure as in the **K-means** case. We obtain an exponential speed-up regarding its classical counterpart in the vector dimensionality  $d$  while maintaining the clustering efficiency.

Finally, we presented the quantum versions of the well-known  $k_T$ -based jet clustering algorithms. They showed an exponential speed-up in the search for the minimum distance. Therefore, while the classical version requires  $\mathcal{O}(N^3)$  in computational cost, the quantum counterpart requires only  $\mathcal{O}(N^2 \log(N))$ . Notice that this comparison is performed between the classical *non-optimal* and not optimized version and its quantum analogue. A fair comparison with the best classical version would require applying to the quantum algorithm at least the geometrical nearest neighbour optimization procedure that is also applied to **FastJet**. In this way, we would obtain a quantum version of order  $\mathcal{O}(N \log(N))$ , which is of the same order as the fully optimal version of **FastJet**.

## Acknowledgements

We thank Abhijat Sharma and Guillermo Alonso for very helpful conversations and suggestions. This work is supported by the Spanish Government (Agencia Estatal de Investigación MCIN/AEI/10.13039/501100011033) Grant No. PID2020-114473GB-I00, and Generalitat Valenciana Grant No. PROMETEO/2021/071. LC is supported by Generalitat Valenciana GenT Excellence Programme (CIDEGENT/2020/011).

## References

- [1] Richard P. Feynman. Simulating physics with computers. *Int. J. Theor. Phys.*, 21:467–488, 1982. doi: 10.1007/BF02650179.
- [2] Lov K. Grover. Quantum mechanics helps in searching for a needle in a haystack. *Phys. Rev. Lett.*, 79:325–328, 1997. doi: 10.1103/PhysRevLett.79.325.
- [3] Peter W. Shor. Polynomial time algorithms for prime factorization and discrete logarithms on a quantum computer. *SIAM J. Sci. Statist. Comput.*, 26:1484, 1997. doi: 10.1137/S0097539795293172.
- [4] Román Orús, Samuel Mugel, and Enrique Lizaso. Quantum computing for finance: Overview and prospects. *Rev. Phys.*, 4:100028, 2019. doi: 10.1016/j.revip.2019.100028.
- [5] Junyu Liu and Yuan Xin. Quantum simulation of quantum field theories as quantum chemistry. *JHEP*, 12:011, 2020. doi: 10.1007/JHEP12(2020)011.
- [6] Eric T. Holland, Kyle A. Wendt, Konstantinos Kravvaris, Xian Wu, W. Erich Ormand, Jonathan L DuBois, Sofia Quaglioni, and Francesco Pederiva. Optimal Control for the Quantum Simulation of Nuclear Dynamics. *Phys. Rev. A*, 101(6):062307, 2020. doi: 10.1103/PhysRevA.101.062307.
- [7] J. E. Lynn, I. Tews, S. Gandolfi, and A. Lovato. Quantum Monte Carlo Methods in Nuclear Physics: Recent Advances. *Ann. Rev. Nucl. Part. Sci.*, 69:279–305, 2019. doi: 10.1146/annurev-nucl-101918-023600.
- [8] Ashley Montanaro. Quantum speedup of Monte Carlo methods. volume 471, page 20150301, 2015. doi: 10.1098/rspa.2015.0301.
- [9] Christian Kokail et al. Self-verifying variational quantum simulation of lattice models. *Nature*, 569(7756):355–360, 2019. doi: 10.1038/s41586-019-1177-4.
- [10] Ryan LaRose, Arkin Tikkun, Étude O’Neel-Judy, Lukasz Cincio, and Patrick J. Coles. Variational quantum state diagonalization. *npj Quantum Information*, 5(1):57, 2019. doi: 10.1038/s41534-019-0167-6. URL <https://doi.org/10.1038/s41534-019-0167-6>.
- [11] Carlos Bravo-Prieto, Diego García-Martín, and José I. Latorre. Quantum singular value decomposer. *Phys. Rev. A*, 101:062310, Jun 2020. doi: 10.1103/PhysRevA.101.062310. URL <https://link.aps.org/doi/10.1103/PhysRevA.101.062310>.
- [12] Andrea Delgado et al. Quantum Computing for Data Analysis in High-Energy Physics. In *2022 Snowmass Summer Study*, 3 2022.
- [13] Richard Keith Ellis et al. Physics Briefing Book: Input for the European Strategy for Particle Physics Update 2020. 10 2019.
- [14] F. Gianotti et al. Physics potential and experimental challenges of the LHC luminosity upgrade. *Eur. Phys. J. C*, 39:293–333, 2005. doi: 10.1140/epjc/s2004-02061-6.
- [15] A. Abada et al. FCC Physics Opportunities: Future Circular Collider Conceptual Design Report Volume 1. *Eur. Phys. J. C*, 79(6):474, 2019. doi: 10.1140/epjc/s10052-019-6904-3.

- [16] The Compact Linear  $e^+e^-$  Collider (CLIC): Physics Potential. 12 2018.
- [17] Mingyi Dong et al. CEPC Conceptual Design Report: Volume 2 - Physics & Detector. 11 2018.
- [18] Annie Y. Wei, Preksha Naik, Aram W. Harrow, and Jesse Thaler. Quantum Algorithms for Jet Clustering. *Phys. Rev. D*, 101(9):094015, 2020. doi: 10.1103/PhysRevD.101.094015.
- [19] Diogo Pires, Pedrame Bargassa, João Seixas, and Yasser Omar. A Digital Quantum Algorithm for Jet Clustering in High-Energy Physics. 1 2021.
- [20] Diogo Pires, Yasser Omar, and João Seixas. Adiabatic Quantum Algorithm for Multijet Clustering in High Energy Physics. 12 2020.
- [21] João Barata and Carlos A. Salgado. A quantum strategy to compute the jet quenching parameter  $\hat{q}$ . *Eur. Phys. J. C*, 81(10):862, 2021. doi: 10.1140/epjc/s10052-021-09674-9.
- [22] Adrián Pérez-Salinas, Juan Cruz-Martinez, Abdulla A. Alhajri, and Stefano Carrazza. Determining the proton content with a quantum computer. *Phys. Rev. D*, 103(3):034027, 2021. doi: 10.1103/PhysRevD.103.034027.
- [23] Christian W. Bauer, Wibe A. de Jong, Benjamin Nachman, and Davide Provasoli. Quantum Algorithm for High Energy Physics Simulations. *Phys. Rev. Lett.*, 126(6):062001, 2021. doi: 10.1103/PhysRevLett.126.062001.
- [24] Simon Williams, Sarah Malik, Michael Spannowsky, and Khadeejah Bepari. A quantum walk approach to simulating parton showers. 9 2021.
- [25] Khadeejah Bepari, Sarah Malik, Michael Spannowsky, and Simon Williams. Towards a quantum computing algorithm for helicity amplitudes and parton showers. *Phys. Rev. D*, 103(7):076020, 2021. doi: 10.1103/PhysRevD.103.076020.
- [26] Wibe A. De Jong, Mekena Metcalf, James Mulligan, Mateusz Płoskoń, Felix Ringer, and Xiaojun Yao. Quantum simulation of open quantum systems in heavy-ion collisions. *Phys. Rev. D*, 104(5):051501, 2021. doi: 10.1103/PhysRevD.104.L051501.
- [27] Wen Guan, Gabriel Perdue, Arthur Pesah, Maria Schuld, Koji Terashi, Sofia Vallecorsa, and Jean-Roch Vlimant. Quantum Machine Learning in High Energy Physics. 5 2020. doi: 10.1088/2632-2153/abc17d.
- [28] Sau Lan Wu et al. Application of quantum machine learning using the quantum variational classifier method to high energy physics analysis at the LHC on IBM quantum computer simulator and hardware with 10 qubits. *J. Phys. G*, 48(12):125003, 2021. doi: 10.1088/1361-6471/ac1391.
- [29] Timo Felser, Marco Trenti, Lorenzo Sestini, Alessio Gianelle, Davide Zuliani, Donatella Lucchesi, and Simone Montangero. Quantum-inspired machine learning on high-energy physics data. *npj Quantum Inf.*, 7(1):111, 2021. doi: 10.1038/s41534-021-00443-w.
- [30] Steve Abel, Juan C. Criado, and Michael Spannowsky. Completely Quantum Neural Networks. 2 2022.

[31] Jack Y. Araz and Michael Spannowsky. Classical versus Quantum: comparing Tensor Network-based Quantum Circuits on LHC data. 2 2022.

[32] Vishal S. Ngairangbam, Michael Spannowsky, and Michihisa Takeuchi. Anomaly detection in high-energy physics using a quantum autoencoder. 12 2021.

[33] Jack Y. Araz and Michael Spannowsky. Quantum-inspired event reconstruction with Tensor Networks: Matrix Product States. *JHEP*, 08:112, 2021. doi: 10.1007/JHEP08(2021)112.

[34] Andrew Blance and Michael Spannowsky. Quantum Machine Learning for Particle Physics using a Variational Quantum Classifier. 10 2020. doi: 10.1007/JHEP02(2021)212.

[35] Stephen P. Jordan, Keith S. M. Lee, and John Preskill. Quantum Algorithms for Quantum Field Theories. *Science*, 336:1130–1133, 2012. doi: 10.1126/science.1217069.

[36] M. C. Bañuls et al. Simulating Lattice Gauge Theories within Quantum Technologies. *Eur. Phys. J. D*, 74(8):165, 2020. doi: 10.1140/epjd/e2020-100571-8.

[37] Erez Zohar, J. Ignacio Cirac, and Benni Reznik. Quantum Simulations of Lattice Gauge Theories using Ultracold Atoms in Optical Lattices. *Rept. Prog. Phys.*, 79(1):014401, 2016. doi: 10.1088/0034-4885/79/1/014401.

[38] Tim Byrnes and Yoshihisa Yamamoto. Simulating lattice gauge theories on a quantum computer. *Phys. Rev. A*, 73:022328, 2006. doi: 10.1103/PhysRevA.73.022328.

[39] Selomir Ramírez-Uribe, Andrés E. Rentería-Olivo, Germán Rodrigo, German F. R. Sborlini, and Luiz Vale Silva. Quantum algorithm for Feynman loop integrals. 5 2021.

[40] Selomir Ramírez-Uribe. Four-loop scattering amplitudes through the loop-tree duality. 12 2021.

[41] S. Lloyd. Least squares quantization in pcm. *IEEE Transactions on Information Theory*, 28 (2):129–137, 1982. doi: 10.1109/TIT.1982.1056489.

[42] Brendan J. Frey and Delbert Dueck. Clustering by passing messages between data points. *Science*, 315:972 – 976, 2007.

[43] S. Catani, Yuri L. Dokshitzer, M. Olsson, G. Turnock, and B. R. Webber. New clustering algorithm for multi - jet cross-sections in e+ e- annihilation. *Phys. Lett. B*, 269:432–438, 1991. doi: 10.1016/0370-2693(91)90196-W.

[44] Matteo Cacciari, Gavin P. Salam, and Gregory Soyez. The anti- $k_t$  jet clustering algorithm. *JHEP*, 04:063, 2008. doi: 10.1088/1126-6708/2008/04/063.

[45] Yuri L. Dokshitzer, G. D. Leder, S. Moretti, and B. R. Webber. Better jet clustering algorithms. *JHEP*, 08:001, 1997. doi: 10.1088/1126-6708/1997/08/001.

[46] Geoffrey H Ball and David J Hall. A clustering technique for summarizing multivariate data. *Behavioral science*, 12(2):153–155, 1967.

[47] James MacQueen et al. Some methods for classification and analysis of multivariate observations. In *Proceedings of the fifth Berkeley symposium on mathematical statistics and probability*, volume 1, pages 281–297. Oakland, CA, USA, 1967.

[48] Petros Drineas, Alan Frieze, Ravindran Kannan, S. Vempala, and V. Vinay. Clustering large graphs via the singular value decomposition: Theoretical advances in data clustering (guest editors: Nina mishra and rajeev motwani). *Machine Learning*, 56, 01 2004. doi: 10.1023/B:MACH.0000033113.59016.96.

[49] David Arthur and Sergei Vassilvitskii. K-means++: The advantages of careful seeding. In *Proceedings of the Eighteenth Annual ACM-SIAM Symposium on Discrete Algorithms*, SODA '07, page 1027–1035, USA, 2007. Society for Industrial and Applied Mathematics. ISBN 9780898716245.

[50] S. Chekanov. A New jet algorithm based on the k-means clustering for the reconstruction of heavy states from jets. *Eur. Phys. J. C*, 47:611–616, 2006. doi: 10.1140/epjc/s2006-02618-3.

[51] Jesse Thaler and Ken Van Tilburg. Maximizing Boosted Top Identification by Minimizing N-subjettiness. *JHEP*, 02:093, 2012. doi: 10.1007/JHEP02(2012)093.

[52] Iain W. Stewart, Frank J. Tackmann, Jesse Thaler, Christopher K. Vermilion, and Thomas F. Wilkason. XCone: N-jettiness as an Exclusive Cone Jet Algorithm. *JHEP*, 11:072, 2015. doi: 10.1007/JHEP11(2015)072.

[53] Matteo Cacciari, Gavin P. Salam, and Gregory Soyez. FastJet User Manual. *Eur. Phys. J. C*, 72:1896, 2012. doi: 10.1140/epjc/s10052-012-1896-2.

[54] Andrew Blance and Michael Spannowsky. Unsupervised event classification with graphs on classical and photonic quantum computers. *JHEP*, 21:170, 2020. doi: 10.1007/JHEP08(2021)170.

[55] Abhijat Sarma, Rupak Chatterjee, Kaitlin Gili, and Ting Yu. Quantum unsupervised and supervised learning on superconducting processors. *Quantum Information and Computation*, 20:541–552, 06 2020. doi: 10.26421/QIC20.7-8-1.

[56] Steph Foulds, Viv Kendon, and Tim Spiller. The controlled SWAP test for determining quantum entanglement. 2021.

[57] Harry Buhrman, Richard Cleve, John Watrous, and Ronald de Wolf. Quantum fingerprinting. *Phys. Rev. Lett.*, 87:167902, Sep 2001. doi: 10.1103/PhysRevLett.87.167902. URL <https://link.aps.org/doi/10.1103/PhysRevLett.87.167902>.

[58] W. Bartel et al. Experimental Evidence for Differences in  $p_T$  Between Quark Jets and Gluon Jets. *Phys. Lett. B*, 123:460–466, 1983. doi: 10.1016/0370-2693(83)90994-2.

[59] S. Bethke, Z. Kunszt, D. E. Soper, and W. James Stirling. New jet cluster algorithms: Next-to-leading order QCD and hadronization corrections. *Nucl. Phys. B*, 370:310–334, 1992. doi: 10.1016/0550-3213(92)90289-N. [Erratum: Nucl.Phys.B 523, 681–681 (1998)].

[60] German Rodrigo, Mikhail S. Bilenky, and Arcadi Santamaria. Quark mass effects for jet production in e+ e- collisions at the next-to-leading order: Results and applications. *Nucl. Phys. B*, 554:257–297, 1999. doi: 10.1016/S0550-3213(99)00293-X.

[61] Seth Lloyd, Masoud Mohseni, and Patrick Rebentrost. Quantum algorithms for supervised and unsupervised machine learning. 2013.

[62] Vittorio Giovannetti, Seth Lloyd, and Lorenzo Maccone. Quantum random access memory. *Physical Review Letters*, 100(16), Apr 2008. ISSN 1079-7114. doi: 10.1103/physrevlett.100.160501. URL <http://dx.doi.org/10.1103/PhysRevLett.100.160501>.

[63] Vittorio Giovannetti, Seth Lloyd, and Lorenzo Maccone. Architectures for a quantum random access memory. *Physical Review A*, 78(5), Nov 2008. ISSN 1094-1622. doi: 10.1103/physreva.78.052310. URL <http://dx.doi.org/10.1103/PhysRevA.78.052310>.

[64] F. De Martini, V. Giovannetti, S. Lloyd, L. Maccone, E. Nagali, L. Sansoni, and F. Sciarrino. Experimental quantum private queries with linear optics, 2009.

[65] I. Chiorescu, N. Groll, S. Bertaina, T. Mori, and S. Miyashita. Magnetic strong coupling in a spin-photon system and transition to classical regime. *Physical Review B*, 82(2), Jul 2010. ISSN 1550-235X. doi: 10.1103/physrevb.82.024413. URL <http://dx.doi.org/10.1103/PhysRevB.82.024413>.

[66] D. I. Schuster, A. P. Sears, E. Ginossar, L. DiCarlo, L. Frunzio, J. J. L. Morton, H. Wu, G. A. D. Briggs, B. B. Buckley, D. D. Awschalom, and R. J. Schoelkopf. High-cooperativity coupling of electron-spin ensembles to superconducting cavities. *Phys. Rev. Lett.*, 105:140501, Sep 2010. doi: 10.1103/PhysRevLett.105.140501. URL <https://link.aps.org/doi/10.1103/PhysRevLett.105.140501>.

[67] Y. Kubo, F. R. Ong, P. Bertet, D. Vion, V. Jacques, D. Zheng, A. Dréau, J.-F. Roch, A. Auffeves, F. Jelezko, J. Wrachtrup, M. F. Barthe, P. Bergonzo, and D. Esteve. Strong coupling of a spin ensemble to a superconducting resonator. *Phys. Rev. Lett.*, 105:140502, Sep 2010. doi: 10.1103/PhysRevLett.105.140502. URL <https://link.aps.org/doi/10.1103/PhysRevLett.105.140502>.

[68] Hua Wu, Richard E. George, Janus H. Wesenberg, Klaus Mølmer, David I. Schuster, Robert J. Schoelkopf, Kohei M. Itoh, Arzhang Ardavan, John J. L. Morton, and G. Andrew D. Briggs. Storage of multiple coherent microwave excitations in an electron spin ensemble. *Phys. Rev. Lett.*, 105:140503, Sep 2010. doi: 10.1103/PhysRevLett.105.140503. URL <https://link.aps.org/doi/10.1103/PhysRevLett.105.140503>.

[69] Christoph Durr and Peter Hoyer. A Quantum algorithm for finding the minimum. 7 1996.

[70] Patrick J. Coles, Stephan J. Eidenbenz, Scott Pakin, Adetokunbo Adedoyin, John Ambrosiano, Petr M. Anisimov, William Casper, Gopinath Chennupati, Carleton Coffrin, Hristo N. Djidjev, David Gunter, Satish Karra, Nathan Lemons, Shizeng Lin, Andrey Y. Lokhov, Alexander Malyzhenkov, David Dennis Lee Mascarenas, Susan M. Mniszewski, Balu Nadiga, Dan O’Malley, Diane Oyen, Lakshman Prasad, Randy Roberts, Philip Romero, Nandakishore Santhi, Nikolai Sinitsyn, Pieter Swart, Marc Vuffray, Jim Wendelberger, Boram Yoon, Richard J. Zamora, and Wei Zhu. Quantum algorithm implementations for beginners. *CoRR*, abs/1804.03719, 2018. URL <http://arxiv.org/abs/1804.03719>.

[71] Richard L Smith. Extreme value theory. *Handbook of applicable mathematics*, 7:437–471, 1990.

[72] E. J. Gumbel. *Statistics of Extremes*. Columbia University Press, 1958. ISBN 9780231891318. doi: doi:10.7312/gumb92958. URL <https://doi.org/10.7312/gumb92958>.

- [73] Thomas M. Reiss R-D. *Statistical Analysis of Extreme Values With Applications to Insurance, Finance, Hydrology and Other Fields*. Birkhauser Verlag, 2007. ISBN 9783764372309.
- [74] Stuart Coles. *An introduction to statistical modeling of extreme values*. Springer Series in Statistics. Springer-Verlag, London, 2001. ISBN 1-85233-459-2.
- [75] Castillo E., Ali S Hadi, Narayanaswamy Balakrishnan, and José-Mariá Sarabia. *Extreme Value and Related Models with Applications in Engineering and Science*. Wiley, 2004. ISBN 9780471671725.
- [76] Dawid Kopczyk. Quantum machine learning for data scientists, 2018.
- [77] Matteo Cacciari and Gavin P. Salam. Dispelling the  $N^3$  myth for the  $k_T$  jet-finder. *Physics Letters B*, 641(1):57–61, Sep 2006. ISSN 0370-2693. doi: 10.1016/j.physletb.2006.08.037. URL <http://dx.doi.org/10.1016/j.physletb.2006.08.037>.
- [78] Marco Fanizza, Andrea Mari, and Vittorio Giovannetti. Optimal Universal Learning Machines for Quantum State Discrimination. *IEEE Transactions on Information Theory*, 65(9):5931–5944, Sep 2019. ISSN 1557-9654. doi: 10.1109/tit.2019.2916646. URL <http://dx.doi.org/10.1109/TIT.2019.2916646>.
- [79] R. Brun and F. Rademakers. ROOT: An object oriented data analysis framework. *Nucl. Instrum. Meth. A*, 389:81–86, 1997. doi: 10.1016/S0168-9002(97)00048-X.

## A Controlled *SwapTest*

A well-known procedure for determining the entanglement between two quantum states is the controlled *SwapTest* [57] method. This method allows us to quantify the overlap between  $|\psi_1\rangle$  and  $|\psi_2\rangle$ , which are two input general quantum states of  $n$  and  $m$  qubits respectively such that  $n \geq m$  (otherwise we exchange the labels 1 and 2), by measuring an ancillary qubit. The controlled *SwapTest* proceeds in three steps starting from the initial state

$$|\Psi_0\rangle = |0, \psi_1, \psi_2\rangle, \quad (20)$$

where the ancillary qubit has been initialized to  $|0\rangle$ . In the first step, a Hadamard ( $H$ ) gate is applied to the ancillary qubit, while the states to be probed are left unchanged, resulting in the new state

$$|\Psi_1\rangle = (H \otimes \mathbf{I}^{\otimes n+m}) |\Psi_0\rangle = \frac{1}{\sqrt{2}} (|0, \psi_1, \psi_2\rangle + |1, \psi_1, \psi_2\rangle), \quad (21)$$

where the identity  $\mathbf{I}^{\otimes n+m}$  acts over the  $|\psi_1\rangle$  and  $|\psi_2\rangle$  states and the tensor product  $\otimes$  is omitted in the composed states (e.g  $|0\rangle \otimes |\psi_1\rangle \otimes |\psi_2\rangle = |0, \psi_1, \psi_2\rangle$ ). A controlled swap gate (CSWAP) is then applied to  $|\Psi_1\rangle$  where all the  $m$  qubits of  $|\psi_2\rangle$  are swapped with the  $m$  first qubits of  $|\psi_1\rangle$ , leading to

$$|\Psi_2\rangle = \text{CSWAP}|\Psi_1\rangle = \frac{1}{\sqrt{2}} (|0, \psi_1, \psi_2\rangle + |1, \psi_2, \psi'_1\rangle), \quad (22)$$

where  $\psi'_i$  is the swapped state of  $\psi_i$ , i.e., a state where the  $m$  first qubits of  $\psi_1$  have been swapped with the rest  $n - m$  qubits. The final step consists of applying again a Hadamard gate to the ancillary qubit

$$|\Psi_3\rangle = (H \otimes \mathbf{I}^{\otimes n+m}) |\Psi_2\rangle = \frac{1}{2} (|0\rangle \otimes (|\psi_1, \psi_2\rangle + |\psi_2, \psi'_1\rangle) + |1\rangle \otimes (|\psi_1, \psi_2\rangle - |\psi_2, \psi'_1\rangle)). \quad (23)$$

The resulting probability of measuring the ancillary qubit in the state  $|0\rangle$  is given by

$$\begin{aligned} P_{\Psi_3}(|0\rangle) &= |\langle 0|\Psi_3\rangle|^2 = \frac{1}{4} |\langle \psi_1, \psi_2 \rangle + \langle \psi_2, \psi'_1 \rangle|^2 = \frac{1}{2} + \frac{1}{2} \text{Re} [\langle \psi_2, \psi'_1 | \psi_1, \psi_2 \rangle] \\ &= \frac{1}{2} + \frac{1}{2} \langle \psi'_1 | \psi_2 \rangle \langle \psi_2 | \psi_1 \rangle, \end{aligned} \quad (24)$$

which turns out to be as follows if  $m = n$ , thus  $|\psi'_1\rangle = |\psi_1\rangle$

$$P_{\Psi_3}(|0\rangle) = \frac{1}{2} + \frac{1}{2} |\langle \psi_1 | \psi_2 \rangle|^2, \quad (25)$$

and this provides the squared inner product between the two states with an uncertainty of  $\mathcal{O}(\epsilon)$  after  $\mathcal{O}(\epsilon^{-2})$  shots. The corresponding quantum circuit associated to the *SwapTest* method is shown in Fig. 8.

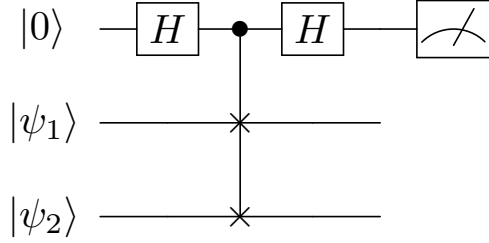


Figure 8: Quantum circuit *SwapTest*.